

# Carbazole isomer induces ultralong organic phosphorescence

Chengjian Chen<sup>1</sup>, Zhenguo Chi<sup>2</sup>, Kok Chan Chong<sup>1</sup>, Andrei S. Batsanov<sup>3</sup>, Zhan Yang<sup>2</sup>, Zhu Mao<sup>2</sup>, Zhiyong Yang<sup>2</sup>, Bin Liu<sup>1,4,\*</sup>

<sup>1</sup>Department of Chemical and Biomolecular Engineering, National University of Singapore, 4 Engineering Drive 4, Singapore 117585, Singapore.

<sup>2</sup>School of Chemistry, Sun Yat-sen University, Guangzhou 510275, China.

<sup>3</sup>Department of Chemistry, Durham University, Durham DH1 3LE, UK.

<sup>4</sup>Joint School of National University of Singapore and Tianjin University, International Campus of Tianjin University, Binhai New City, Fuzhou 350207, China

\*Corresponding author. Email: cheliub@nus.edu.sg

**Commercial carbazole (Cz) has been widely used to synthesize organic functional materials that have led to recent breakthroughs in ultralong organic phosphorescence<sup>1</sup>, thermally activated delayed fluorescence<sup>2,3</sup>, organic luminescent radicals<sup>4</sup> and organic semiconductor lasers<sup>5</sup>. However, the impact of low concentration isomeric impurities present in commercial batches on the properties of the synthesized molecules requires further analysis. Here, we synthesized highly pure Cz (Lab-Cz), and observed that its fluorescence is blue-shifted by 54 nm with respect to commercial samples whereas its room-temperature ultralong phosphorescence almost disappears<sup>6</sup>. We discover that such differences are due to the presence of a Cz isomeric impurity in commercial Cz sources, with concentration <0.5 mol%. Ten representative Cz derivatives resynthesized from the Lab-Cz failed to show the ultralong phosphorescence reported in previous literature<sup>1,7-15</sup>. However, phosphorescence is recovered by adding 0.1 mol% isomers, which act as charge traps. Investigating the role of isomers can therefore provide alternative insight on the mechanisms behind ultralong organic phosphorescence<sup>1,6-18</sup>.**

Ultralong phosphorescence, also called afterglow, is resulted from the storage of excitation energy and slow release of luminescence mainly *via* triplet states<sup>19,20</sup>. The first scientifically documented afterglow material was Bologna Stone and its afterglow was caused by impurity doping<sup>21</sup>. Two decades ago, the research interest of inorganic afterglow was heated up by doping Dy<sup>3+</sup> into the SrAl<sub>2</sub>O<sub>4</sub>:Eu<sup>2+</sup> phosphor<sup>22</sup>. Nowadays, inorganic afterglow has been extensively employed to produce luminous paints, dials, emergency signs and so on<sup>19</sup>. As compared to the inorganic counterpart, organic materials show more advantages, such as flexibility, transparency, solubility and color tunability<sup>20</sup>. Recently, organic afterglow materials including carbazole, dibenzothiophene, dibenzofuran, fluorene and their derivatives have been successfully developed<sup>14</sup>. However, their impurity hypotheses have been under debate since the early 20<sup>th</sup> century<sup>6,15,23</sup>, but without solid evidence. For example, through sublimation and recrystallization, small traces of impurities were proposed to contribute to phosphorescence<sup>23</sup>, while the impurity effect was ruled out by the explanation of crystal quality nearly 40 years later<sup>6</sup>. Notably, the phosphorescence of many solid organic compounds was attributed to very small traces of impurities<sup>15,23</sup>. Therefore, identifying the molecular structure of impurity conundrum is critical to build frameworks for efficient utilization of triplet states in organic functional materials.

42 More than a century ago, carbazole (Cz) was successfully isolated from the anthracene  
43 fraction of coal tar<sup>24</sup>, which is the current commercial source of Cz. During the past 5 years, Cz  
44 derivatives have attracted much research interest, and many of them have directly led to the  
45 recent breakthroughs, such as highly efficient delayed fluorescence emitters<sup>2,3</sup>, efficient organic  
46 luminescent radicals<sup>4</sup> and organic semiconductor lasers<sup>5</sup>. In particular, commercial Cz  
47 derivatives are the current focus of single-component organic ultralong phosphorescence  
48 studies<sup>1,6-14,16-18</sup>. However, fundamental inconsistencies emerged when the same compounds  
49 were repeatedly reported by different research groups<sup>7-12,15</sup>. We therefore examined the  
50 commercial Cz from Tokyo Chemical Industry (TCI), J&K, Sigma-Aldrich (Sigma) and  
51 Aladdin. All of them showed room-temperature ultralong phosphorescence after  
52 recrystallization<sup>6</sup>, but with varied intensities and durations. Moreover, we also tried to purify Cz  
53 of TCI (TCI-Cz) using column chromatography three times with dichloromethane/hexane (1/3,  
54 v/v), ether acetate/hexane (5/95, v/v) and dichloromethane/hexane (1/2, v/v) as the eluents,  
55 respectively, which was followed by recrystallization from toluene. The obtained TCI-Cz still  
56 showed very bright room-temperature ultralong phosphorescence, clearly visible to naked eye.

57 We then synthesized Cz (Lab-Cz) from 2-aminobiphenyl (details in Methods).  
58 Surprisingly, the fluorescence of Lab-Cz is blue-shifted by 54 nm (Supplementary Fig. 1) and the  
59 well-known ultralong phosphorescence almost disappears as compared to that for TCI-Cz in the  
60 same crystal state (Fig. 1a)<sup>6,8</sup>. Notably, the room-temperature ultralong phosphorescence of Lab-  
61 Cz crystals could not be observed by naked eye. However, as shown in Supplementary Fig. 2,  
62 very weak luminescence from Lab-Cz could be captured by a Sony camera at 8.3 ms off 365 nm  
63 light illumination, and the signal disappeared after 83.3 ms. Under the same camera setting, the  
64 photos of TCI-Cz were all overexposed with strong luminescent and background signals. This  
65 result indicates that some small traces of impurities play a key role in ultralong phosphorescence.

66 To separate the impurities, many methods had been tried without success until high-  
67 performance liquid chromatography (HPLC) was rationalized to monitor the onset absorption at  
68 346 nm. This wavelength was essential because when monitored at 294 nm (Fig. 1b), the signal  
69 of impurity was easily covered by the maximum absorption of the dominant Cz (Supplementary  
70 Fig. 3). However, at the onset absorption of 346 nm (Fig. 1c), the impurity peak is uncovered  
71 gradually when optimizing acetonitrile-water ratio from 95/5 to 50/50 (v/v). After isolating ~10  
72 mg of the impurity from commercial TCI-Cz (details in Supplementary Methods), X-ray  
73 crystallography revealed its structure as an isomer of Cz, 1*H*-benzo[*f*]indole (Bd, Fig. 1c and  
74 Supplementary Fig. 4a). The isomer Bd itself does not show room-temperature ultralong  
75 phosphorescence even in the crystal state. We further identified the same impurity from Cz  
76 supplied by J&K, Sigma-Aldrich and Aladdin, but with different content (Figs. 1d, 2a and  
77 Supplementary Table 1). As the isomer Bd inherits similar reactivity to Cz, we speculate that this  
78 widespread isomer could affect a variety of organic materials derived from commercial Cz.

79 Taking CPhCz and DPhCzT (Figs. 2c, d) as the examples<sup>1,7</sup>, the contribution of Bd to their  
80 reported ultralong phosphorescence was studied in detail. Considering Bd in commercial Cz  
81 (Fig. 2a), TCI-CPhCz (synthesized from TCI-Cz) was carefully purified by column three times  
82 before recrystallization (details in Supplementary Methods). In the same single crystal state (Fig.  
83 2d), the purified TCI-CPhCz exclusively shows room-temperature ultralong phosphorescence in  
84 contrast to Lab-CPhCz (synthesized from Lab-Cz). Meanwhile, the optimized HPLC of the  
85 recrystallized TCI-CPhCz revealed a small trace of impurity upon monitoring at the onset  
86 absorption of 354 nm, which was later quantified to be 0.1 mol% (Fig. 2b). X-ray

87 crystallography identified its structure as CPhBd (Fig. 2c and Supplementary Fig. 4b), after  
88 isolating ~22 mg of the impurity from TCI-CPhCz. CPhBd itself does not show room-  
89 temperature ultralong phosphorescence in the crystal state. We further confirmed that CPhBd  
90 could be scaled up from Bd by using the same synthetic method as that of CPhCz from Cz  
91 (Supplementary Scheme 1)<sup>7</sup>. Similarly, following the procedure for DPhCzT from Cz<sup>1</sup>, DPhBdT  
92 (Fig. 2c) was synthesized from Bd and no room-temperature ultralong phosphorescence was  
93 observed by naked eye.

94 To explore the generality of the phenomenon, another 8 representative Cz derivatives with  
95 reported ultralong phosphorescence were further tested (Supplementary Fig. 5)<sup>1,7-15</sup>. It was found  
96 that their reported ultralong phosphorescence was only observed by naked eye with the crystals  
97 synthesized from TCI-Cz, but not from Lab-Cz. Taken together, we propose that the isomer Bd  
98 in commercial Cz is responsible for their reported ultralong phosphorescence. This result also  
99 indicates that the widespread presence of Bd should be taken into consideration for other organic  
100 semiconductors directly synthesized from commercial Cz without proper exclusion of the isomer  
101 especially for those being used in optoelectronic applications<sup>2-5,25</sup>. The ultralong  
102 phosphorescence of Bd/Lab-Cz could be observed even at the presence of 0.01 mol% Bd  
103 (Supplementary Fig. 6b), implying that the isomer doping is extremely effective. This ultra-low  
104 content also explains why the impurity effect has been largely ignored so far<sup>1,6-14</sup>.

105 To understand how the isomer affects ultralong phosphorescence, emission characteristics  
106 were investigated with 0 mol%, 0.5 mol%, 1 mol%, 5 mol%, 10 mol% and 100 mol% isomer  
107 dopants in crystalline states, respectively (Fig. 3 and Supplementary Fig. 7). The isomer doping  
108 effect of ultralong phosphorescence could be further corroborated since each pair of 0.5 mol%  
109 Bd/Lab-Cz and TCI-Cz (Fig. 3a), 0.5 mol% CPhBd/CPhCz and TCI-CPhCz (Fig. 3b), 0.5 mol%  
110 DPhBdT/DPhCzT and TCI-DPhCzT (Fig. 3c), respectively, shows nearly identical prompt and  
111 delayed spectra. More importantly, even with 0.1 mol% isomer doping, the above doping  
112 systems show effective room-temperature ultralong phosphorescence (Supplementary Fig. 6).  
113 Meanwhile, the phosphorescent emission from crystalline powders was stable in air  
114 (Supplementary Fig. 8) and their doped polymer films also showed room-temperature ultralong  
115 phosphorescence (Supplementary Fig. 9).

116 As for the the prompt emission (Figs. 3d-f), the fluorescence of Bd/Lab-Cz, CPhBd/CPhCz  
117 and DPhBdT/DPhCzT is red-shifted with increasing dopant content, implying that Lab-Cz could  
118 benefit the development of deep-blue emitters as compared to those based on commercial Cz<sup>25</sup>.  
119 Moreover, the distinct differences (solid lines in Figs. 3d-f) between the prompt emissions from  
120 each pair of isomers indicate that Cz and Bd own totally different electron-donating capabilities.  
121 In addition, the well-resolved fluorescence in Figs. 3d and f indicates that the emissions are from  
122 the local-excited (LE) states, while the broad fluorescence in Fig. 3e is the characteristic of  
123 charge-transfer (CT) emission<sup>18,26</sup>.

124 Figure 3g shows the delayed LE emission of Bd/Lab-Cz, with one band at 364-543 nm and  
125 the other newly generated band at 544-836 nm after 8 ms delay upon photoexcitation at room-  
126 temperature. The delayed component of the short wavelength band varies with the dopant  
127 concentration, which agrees with the prompt emission (dashed lines in Fig. 3d), indicating that  
128 the fluorescence of Bd is involved in the delayed emission. The long wavelength band shows the  
129 highest intensity of delayed emission at 1 mol% doping. A similar phenomenon of LE delayed  
130 emission is observed for DPhBdT/DPhCzT (Fig. 3i). For CPhBd/CPhCz in Fig. 3h, the  
131 negligible CT delayed emission and obvious LE delayed emission with a maximum at 5 mol%

132 should be resulted from CT to LE intersystem crossing<sup>26,27</sup>. The delayed emission characteristics  
133 indicate that singlet and triplet excited states are simultaneously generated (Supplementary Fig.  
134 10). Furthermore, the representative photographs of the isomer doping with varying  
135 concentrations are shown in Figs. 3j-l.

136 Room-temperature ultralong phosphorescence based on the isomer doping differs from  
137 most design paradigms<sup>1,7-9,14,15,17,20,28</sup>. The very similar molecular structure and size  
138 (Supplementary Fig. 11) allow the isomers to interact tightly<sup>28</sup> and generate beneficial defects to  
139 store excitation energy. To explore the mechanism, transient absorption was obtained by using  
140 the absorbance spectrum at 8 ms after photo-excitation minus that before photo-excitation<sup>20</sup>, so  
141 that the delayed emission (negative absorption) and transient absorption (positive absorption)  
142 spectra were synchronously recorded in Figs. 4a-c and Supplementary Fig. 12. The broad  
143 absorption bands with peaks located at 460-475 nm were ascribed to radical ions<sup>20</sup>, which were  
144 generated from charge separation. Without doping (black lines in Figs. 4a-c), spectra traced noise  
145 with photoexcitation ceased after 8 ms, indicating that charge-separated states were not  
146 generated in the Lab-Cz, Lab-CPhCz and Lab-DPhCzT crystals. Therefore, their reported  
147 ultralong phosphorescence was not observed by naked eye (Figs. 1a, 2d and 3g-i)<sup>1,6,7</sup>. While with  
148 doping (coloured lines in Figs. 4a-c), delayed emission and transient absorption of charge-  
149 separated states were simultaneously captured, indicating that ultralong phosphorescence was  
150 resulted from charge-separated states<sup>20</sup>. Further comparing 5 mol% CPhBd/CPhCz with CPhBd  
151 (Supplementary Fig. 13a), transient absorption spectra from 8 ms to 1 s show that the absorption  
152 and emission intensities are decreasing simultaneously with time, while the noise spectrum of  
153 CPhBd at 8 ms delay after photoexcitation implies no charge-separated states in the CPhBd  
154 crystals.

155 Owing to the different electron-donating capabilities, Cz and Bd moieties in close  
156 proximity could act as a micro planar heterojunction to generate photoinduced charge-separated  
157 states. To validate our hypothesis, we designed the 5 mol% cross doping systems of Bd/CPhCz,  
158 Bd/DPhCzT, CPhBd/Cz and DPhBdT/Cz. By comparing the prompt emission at 77 K with the  
159 delayed emission at room-temperature (Fig. 4d), the 5 mol% cross doping systems were found to  
160 emit ultralong phosphorescence with peaks located at 525-675 nm, which were from the newly  
161 generated charge-separated states (Supplementary Fig. 13b). The photographs of their ultralong  
162 phosphorescence are shown in Fig. 4e.

163 To further elucidate the mechanism, we studied the simple Bd/Cz doping system as an  
164 example (Fig. 4f). The highest occupied molecular orbital (HOMO) and lowest unoccupied  
165 molecular orbital (LUMO) energy levels were calculated from Supplementary Fig. 14. During  
166 photoexcitation, two types of charge transfer could occur between Bd and Cz, inducing the  
167 generation of Cz radical anions (Supplementary Fig. 15) and Bd radical cations<sup>20</sup>. Meanwhile,  
168 the Cz radical anions diffuse in the crystals and the Bd radical cations are trapped by defects,  
169 forming charge-separated states. Consequently, ultralong phosphorescence is resulted from  
170 gradual charge recombination of charge-separated states in the trap-detrap model of defects.

171 In summary, comparison between lab-synthesized and commercial sources of Cz, followed  
172 by optimization of HPLC offers a feasible solution to the impurity conundrums, which is  
173 applicable to other systems, such as commercial dibenzothiophene and dibenzofuran  
174 (Supplementary Fig. 16). Our studies reveal that the widespread isomer Bd in commercial Cz can  
175 be synchronously derived into many organic functional materials, which forms the isomer  
176 doping systems to activate ultralong phosphorescence. The identification of Bd molecular

177 structure opens completely different molecular design principles to manage triplet states in  
178 developing organic functional materials. This discovery also drives us to design and study the  
179 isomer effect on various organic functional materials, which is on-going in our lab.

## 180 **References**

- 181 1. An, Z. et al. Stabilizing triplet excited states for ultralong organic phosphorescence. *Nat.*  
182 *Mater.* **14**, 685-690 (2015).
- 183 2. Uoyama, H., Goushi, K., Shizu, K., Nomura, H. & Adachi, C. Highly efficient organic light-  
184 emitting diodes from delayed fluorescence. *Nature* **492**, 234-238 (2012).
- 185 3. Hamze, R. et al. Eliminating nonradiative decay in Cu(I) emitters: >99% quantum efficiency  
186 and microsecond lifetime. *Science* **363**, 601-606 (2019).
- 187 4. Ai, X. et al. Efficient radical-based light-emitting diodes with doublet emission. *Nature* **563**,  
188 536-540 (2018).
- 189 5. Sandanayaka, A. S. D. et al. Indication of current-injection lasing from an organic  
190 semiconductor. *Appl. Phys. Express* **12**, 061010 (2019).
- 191 6. Bilen, C. S., Harrison, N. & Morantz, D. J. Unusual room temperature afterglow in some  
192 crystalline organic compounds. *Nature* **271**, 235-237 (1978).
- 193 7. Cai, S. et al. Visible-light-excited ultralong organic phosphorescence by manipulating  
194 intermolecular interactions. *Adv. Mater.* **29**, 1701244 (2017).
- 195 8. Xie, Y., Ge, Y., Peng, Q., Li, C., Li, Q. & Li, Z. How the molecular packing affects the room  
196 temperature phosphorescence in pure organic compounds: ingenious molecular design,  
197 detailed crystal analysis, and rational theoretical calculations. *Adv. Mater.* **29**, 1606829  
198 (2017).
- 199 9. Xiong, Y. et al. Designing efficient and ultralong pure organic room-temperature  
200 phosphorescent materials by structural isomerism. *Angew. Chem. Int. Ed.* **57**, 7997-8001  
201 (2018).
- 202 10. Zhang, T., Wang, X., An, Z., Fang, Z., Zhang, Y. & Yuan, W. Z. Pure organic persistent  
203 room-temperature phosphorescence at both crystalline and amorphous states.  
204 *ChemPhysChem* **19**, 2389-2396 (2018).
- 205 11. Gong, Y. et al. Achieving persistent room temperature phosphorescence and remarkable  
206 mechanochromism from pure organic luminogens. *Adv. Mater.* **27**, 6195-6201 (2015).
- 207 12. Yang, Z. et al. Intermolecular electronic coupling of organic units for efficient persistent  
208 room-temperature phosphorescence. *Angew. Chem. Int. Ed.* **55**, 2181-2185 (2016).
- 209 13. Fateminia, S. M. A., Mao, Z., Xu, S., Yang, Z., Chi, Z. & Liu, B. Organic nanocrystals with  
210 bright red persistent room-temperature phosphorescence for biological applications. *Angew.*  
211 *Chem. Int. Ed.* **56**, 12160-12164 (2017).
- 212 14. Kenry, Chen, C. & Liu, B. Enhancing the performance of pure organic room-temperature  
213 phosphorescent luminophores. *Nat. Commun.* **10**, 2111 (2019).
- 214 15. Xue, P. et al. Correction: Bright persistent luminescence from pure organic molecules  
215 through a moderate intermolecular heavy atom effect. *Chem. Sci.* **8**, 6691-6691 (2017).
- 216 16. Gu, L. et al. Dynamic ultralong organic phosphorescence by photoactivation. *Angew. Chem.*  
217 *Int. Ed.* **57**, 8425-8431 (2018).
- 218 17. Zhao, W. et al. Boosting the efficiency of organic persistent room-temperature  
219 phosphorescence by intramolecular triplet-triplet energy transfer. *Nat. Commun.* **10**, 1595  
220 (2019).
- 221 18. Mao, Z. et al. Two-photon-excited ultralong organic room temperature phosphorescence by  
222 dual-channel triplet harvesting. *Chem. Sci.* **10**, 7352-7357 (2019).

- 223 19. Li, Y., Gecevicius, M. & Qiu, J. Long persistent phosphors—from fundamentals to  
224 applications. *Chem. Soc. Rev.* **45**, 2090-2136 (2016).
- 225 20. Kabe, R. & Adachi, C. Organic long persistent luminescence. *Nature* **550**, 384-387 (2017).
- 226 21. Lastusaari, M. et al. The bologna stone: history's first persistent luminescent material. *Eur. J.*  
227 *Mineral* **24**, 885-890 (2012).
- 228 22. Matsuzawa, T., Aoki, Y., Takeuchi, N. & Murayama, Y. A new long phosphorescent  
229 phosphor with high brightness, SrAl<sub>2</sub>O<sub>4</sub>:Eu<sup>2+</sup>, Dy<sup>3+</sup>. *J. Electrochem. Soc.* **143**, 2670-2673  
230 (1996).
- 231 23. Clapp, D. B. The phosphorescence of tetraphenylmethane and certain related substances. *J.*  
232 *Am. Chem. Soc.* **61**, 523-524 (1939).
- 233 24. Graebe, C. & Glaser, C. *Ber. Dtsch. Chem. Ges.* **5**, 12 (1872).
- 234 25. Feng, H., Zeng, J., Yin, P. et al. Tuning molecular emission of organic emitters from  
235 fluorescence to phosphorescence through push-pull electronic effects. *Nat. Commun.* **11**,  
236 2617 (2020).
- 237 26. Chen, C. et al. Intramolecular charge transfer controls switching between room temperature  
238 phosphorescence and thermally activated delayed fluorescence. *Angew. Chem. Int. Ed.* **57**,  
239 16407-16411 (2018).
- 240 27. Noda, H. et al. Critical role of intermediate electronic states for spin-flip processes in charge-  
241 transfer-type organic molecules with multiple donors and acceptors. *Nat. Mater.* **18**, 1084-  
242 1090 (2019).
- 243 28. Bolton, O., Lee, K., Kim, H.-J., Lin, K. Y. & Kim, J. Activating efficient phosphorescence  
244 from purely organic materials by crystal design. *Nat. Chem.* **3**, 205-210 (2011).

## 245 **Acknowledgments**

246 This study was supported by the Singapore National Research Foundation (NRF) Competitive  
247 Research Program (R279-000-483-281), NRF Investigatorship (R279-000-444-281) and  
248 National University of Singapore (R279-000-482-133).

## 249 **Author contributions**

250 C.C. and B.L. designed the experiments. C.C. optimized HPLC and grew crystals. C.C., Z.C.,  
251 Z.Y., Z.M. and Z.Y. contributed to optical characterizations. C.C. and K.C.C. synthesized all  
252 compounds. A.S.B. and C.C. solved crystal structures. C.C. and B.L. discussed the results and  
253 drafted the manuscript. B.L. supervised the project. All authors contributed to the proofreading.

## 254 **Competing interests**

255 The authors declare no competing interests.

## 256 **Additional information**

257 **Supplementary information** is available online.

258 **Reprints and permissions information** is available at [www.nature.com/reprints](http://www.nature.com/reprints).

259 **Correspondence and requests for materials** should be addressed to B.L.

260

261

262

263

264

265 **Fig. 1 | Paradox of ultralong phosphorescence carbazole.** **a**, Photographs of TCI-Cz and Lab-  
266 Cz crystals at daylight, 365 nm irradiation ON/OFF, and their single crystal structures with unit  
267 cell parameters. **b,c**, HPLC spectra of TCI-Cz crystals monitored at 294 and 346 nm with 95/5 to  
268 50/50 acetonitrile (ACN)-water ratio (v/v) and chemical structures of Cz and Bd. **d**, The  
269 commercial source (e.g. TCI, J&K, SIGMA-ALDRICH, aladdin) of Cz, mixed with its isomer of  
270 Bd.

271

272 **Fig. 2 | Impurity effect on carbazole derivatives.** **a,b**, HPLC spectra monitored at the onset  
273 absorption of 346 nm for Cz (**a**) and 354 nm for CPhCz (**b**) from commercial and lab-  
274 synthesized sources, respectively. The elapsed time aberrations caused by injections were shifted  
275 by setting Lab-Cz and Lab-CPhCz as the reference, respectively. **c**, Chemical structures of  
276 CPhCz, CPhBd, DPhCzT and DPhBdT. **d**, Photographs of CPhCz and DPhCzT crystalline  
277 powders at daylight, 365 nm irradiation ON/OFF, and their single crystal structures with unit cell  
278 parameters. TCI-CPhCz and TCI-DPhCzT were synthesized from TCI-Cz. Lab-CPhCz and Lab-  
279 DPhCzT were synthesized from Lab-Cz.

280

281 **Fig. 3 | Emission characteristics with different isomer doping concentrations.** **a-c**,  
282 Photoluminescence (PL) spectra of crystalline powders resolved into components of prompt and  
283 delayed 8ms at room-temperature (RT) in air; 0.5 mol% Bd/Lab-Cz and TCI-Cz (**a**), 0.5 mol%  
284 CPhBd/CPhCz and TCI-CPhCz (**b**), 0.5 mol% DPhBdT/DPhCzT and TCI-DPhCzT (**c**). **d-f**,  
285 Prompt components of 0 mol%, 0.5 mol%, 1 mol%, 5 mol%, 10 mol% and 100 mol% isomer  
286 dopants; Bd/Lab-Cz (**d**), CPhBd/CPhCz (**e**) and DPhBdT/DPhCzT (**f**). **g-i**, Delayed 8 ms  
287 components of 0 mol%, 0.5 mol%, 1 mol%, 5 mol%, 10 mol% and 100 mol% isomer dopants  
288 after 365 nm excitation off; Bd/Lab-Cz (**g**), CPhBd/CPhCz (**h**) and DPhBdT/DPhCzT (**i**). **j-l**,  
289 Photographs of crystalline powders with 0.5 mol%, 1 mol%, 5 mol% and 10 mol% isomer  
290 dopants of Bd/Cz (**j**), CPhBd/CPhCz (**k**) and DPhBdT/DPhCzT (**l**). 310 nm excitation was used  
291 for the prompt spectra in **a,c,d** and 365 nm excitation for all other measurements.

292

293 **Fig. 4 | Transient absorption, PL and ultralong phosphorescence mechanism. a-c,**  
294 Photoinduced transient absorption (TA) of crystalline powders with 0 mol%, 1 mol%, 5 mol%  
295 and 10 mol% isomer dopants; Bd/Lab-Cz (**a**), CPhBd/CPhCz (**b**) and DPhBdT/DPhCzT (**c**). **d,**  
296 Emission of prompt at 77 K and delayed 8 ms at RT with 5 mol% cross doping systems of  
297 Bd/CPhCz, Bd/DPhCzT, CPhBd/Cz and DPhBdT/Cz crystalline powders. **e,** Photographs of  
298 crystalline powders under 365 nm ON, OFF, OFF 0.2 s and OFF 1 s. **f,** Proposed mechanism of  
299 ultralong phosphorescence (Phos.) with Bd/Cz as an example. Left, charge transfer during  
300 photoexcitation; *Type I*, electrons from the LUMO of Bd are transferred to the LUMO of Cz;  
301 *Type II*, electrons from the HOMO of Bd are transferred to the HOMO of Cz. Middle, charge-  
302 separated states are formed with Cz radical anions diffusing to the neighbour Cz, while Bd  
303 radical cations are trapped by the defects. Note that the intrinsic lattice defects may occur  
304 spontaneously during crystal growth. Right, singlets (e.g.  $S_1$ ) and triplets (e.g.  $T_1$ ) are generated  
305 from the charge recombination (CR) and intersystem crossing (ISC) of  $S_1$  to  $T_1$  is enabled.

## 307 Methods

308 The syntheses, isolation of Bd from TCI-Cz, preparation of doping systems and polymer films, growth of single  
309 crystals, photographs and time-dependent density functional theory (TD-DFT) calculations are fully described in  
310 Supplementary Methods (see Supplementary Information).

311 **Materials.** Commercial carbazoles were obtained from TCI (Product of Japan, C0032-100 g), J&K (Product of  
312 Beijing, 601413-250 g), Sigma-Aldrich (Product of Germany, C5132-100 g), and Aladdin (Product of Shanghai,  
313 C104875-100 g), and were further recrystallized from toluene before using. After customized synthesis from Arch  
314 Bioscience Company, Bd was further purified by column (5/95, v/v, EA/hexane) and then recrystallized from  
315 hexane. White sheet crystals were obtained (~5%, total purification yield), which have a different odor from Lab-Cz.  
316 Commercial dibenzothiophene was purchased from Sigma-Aldrich (Product of Belgium, D32202-25 g).  
317 Commercial dibenzofuran was purchased from TCI (Product of Japan, D0147-25 g). 2-Aminobiphenyl was  
318 purchased from Combi-Blocks (Product of USA, QS7870-25 g). Biphenyl-2-thiol was ordered from ChemCollect  
319 GmbH (Product of Germany, ChemCol-DP000316-5 g). Tetrahydrofuran (THF) was distilled with sodium and  
320 benzophenone. All solvents were HPLC grade from Fisher Chemical unless noted, and ultra-pure water was  
321 produced by SMART2PURE of ThermoFisher Scientific. All other chemicals were obtained from commercial  
322 sources and directly used as received unless noted.

323 **Synthesis of Lab-Cz<sup>29,30</sup> (Supplementary Scheme 1).** 2-Aminobiphenyl (0.85g, 5.0 mmol) was dissolved in a  
324 degassed solution containing 6.0 mL of ultra-pure water and 1.0 mL of concentrated sulfuric acid at 50 °C. After  
325 stirring at 50 °C for 5 min, the resulting solution was cooled to 0 °C in an ice-water bath, and a solution of 0.42 g  
326 (6.1 mmol) of sodium nitrite in 4.7 mL of ultra-pure water was added dropwise. The solution was stirred in the ice-  
327 water bath for 30 min. A solution of 0.56 g (8.6 mmol) of sodium azide in 3.5 mL of ultra-pure water was added  
328 dropwise into the cold solution and the mixture was further stirred for 1 h. The mixture was then filtered and washed  
329 with 100 mL of 2 M potassium carbonate solution for 3 times and then with 300 mL of ultra-pure water for 5 times.  
330 Afterward, the filtrate was dissolved with dichloromethane (DCM) and purified using column chromatography with  
331 DCM/hexane (1/3, v/v) as the eluent to yield 2-azidobiphenyl as a light-yellow oil (0.94 g, 4.8 mmol, 96% yield).  
332 The above procedures were repeated several times to produce sufficient amount of 2-azidobiphenyl.

333  
334 2-Azidobiphenyl (4.0 g, 23.7 mmol) was then dissolved in 60 mL of acetone and added into a mixture containing  
335 100 mL of acetone and 100 mL of ultra-pure water. 5.0 g of silica gel was subsequently added to the mixture and  
336 stirred for 24 h under the illumination of two HITACHI F6T5 6W fluorescent lamps, which changed the mixture  
337 from colourless to brown. The detailed setup for this photochemical step is shown in the Supplementary Fig. 17.  
338 Furthermore, the reaction solvent (260 mL) was maintained by adding acetone every 8 h. The whole reaction was  
339 covered by tinfoil. After removing the solvent by rotary evaporator, the mixture was purified using column  
340 chromatography with DCM/hexane (1/3, v/v) as the eluent. The white powder of carbazole was further purified  
341 using column chromatography two more times with ethyl acetate/hexane (5/95, v/v) and DCM/hexane (1/2, v/v) as

342 the eluent, respectively. After 3 times of column purification, the product was recrystallized from toluene to yield  
343 carbazole (1.2 g, 7.2 mmol, 30% yield) as white sheet crystals. The melting point of Lab-Cz was 246.9 °C and its  
344 comparison with commercial carbazole is listed in Supplementary Fig. 18.

345 **General.** HPLC purifications were conducted by using XBridge® Prep C18 OBD™ 5 µm, 50 mm × 150 mm  
346 column with 20.00 mL/min based on Waters 2545 Binary Gradient Module, Waters 2707 Autosampler and Waters  
347 Fraction Collector III. Injection volume for Cz purification was 1500 µL each at 10.0 mg/mL and injection volume  
348 for CPhCz purification was 1700 µL each at 4.0 mg/mL. DPhCzT was not sufficiently soluble in methanol or ACN  
349 and hence it could not reveal the impurity peak by HPLC based on C18 column. Purifications with silica gel column  
350 chromatography were performed using DAVISIL® silica LC60A 40-63 micro purchased from GRACE and  
351 monitored by TLC silica gel plates with 0.2-0.25 mm coating thickness from SANPONT. NMR spectra were  
352 performed with a Bruker Avance-III 400 NanoBay HD NMR spectrometer at ambient temperature. High-resolution  
353 mass spectrometry (HRMS) was investigated with a Bruker AmaZon X LC-MS for electrospray ionization. Cyclic  
354 voltammetry was performed to calculate HOMO<sup>26</sup> by BioLogic VMP-300 in a DCM (99.9%, Super Dry, stabilized,  
355 J&K Seal) solution containing 5×10<sup>-4</sup> M sample and 0.1 M Bu<sub>4</sub>NPF<sub>6</sub> electrolyte. Electrodes: working (glassy  
356 carbon), counter (Pt disk), reference (Ag/AgCl, calibrated against ferrocene), 100 mV·s<sup>-1</sup>. LUMO was determined by  
357 further measuring ultraviolet/visible absorption with Hitachi U-3900. Melting point (Mpt) was measured with  
358 differential scanning calorimetry (DSC). The instrument model was NETZSCH DSC 204 F1 Phoenix. 10 K/min was  
359 used for the heating procedure under the protection of nitrogen. Mpt was recorded with the DSC curves from the  
360 second heating process. The Mpts were the onset values, which were determined by 'NETZSCH Proteus Thermal  
361 Analysis' software. UV-visible absorption spectra of solution and solid were performed on Shimadzu UV-1700 and  
362 UV-3600 ultraviolet-visible-near-infrared (UV-Vis-NIR) spectrometers, respectively. X-ray diffraction experiments  
363 were carried out on a 4-circle goniometer Kappa geometry Bruker D8 Venture diffractometer with a PHOTON 100  
364 CMOS active pixel sensor detector.

365  
366 **Optical measurements.** PL spectra of 5 mol% Bd/Lab-Cz, 5 mol% CPhBd/CPhCz and 5 mol% DPhBdT/DPhCzT  
367 crystalline powders in air and vacuum were measured by Edinburgh FLS980 using OXFORD Optistat DN as the  
368 sample holder. After vacuum-pumping for 30 min, the emission of crystalline samples in vacuum was measured.  
369 Transient decay spectra, temperature-dependent photoluminescence spectra and PL quantum yield (PLQY) were  
370 carried out using a Jobin Yvon-Horiba FL-3 spectrofluorometer and equipped with a calibrated integrating sphere.  
371 Notably, PLQY of these doping systems was randomly fluctuant, which was probably caused by the emission  
372 intensity changes with prolonging the photo-irradiation<sup>16</sup>, and hence the PLQY was not reported here. Time-  
373 resolved PL spectra (room-temperature and 77 K)<sup>18</sup> and photo-induced transient absorption spectra<sup>20</sup> were obtained  
374 at ambient temperature in air through Ocean Optics QE65 Pro CCD with Ocean Optics LED-365 and LED-310 as  
375 excitation sources and Ocean Optics DH-2000-BAL as UV-VIS-NIR light source, which were assembled according  
376 to the references.

## 378 Data availability

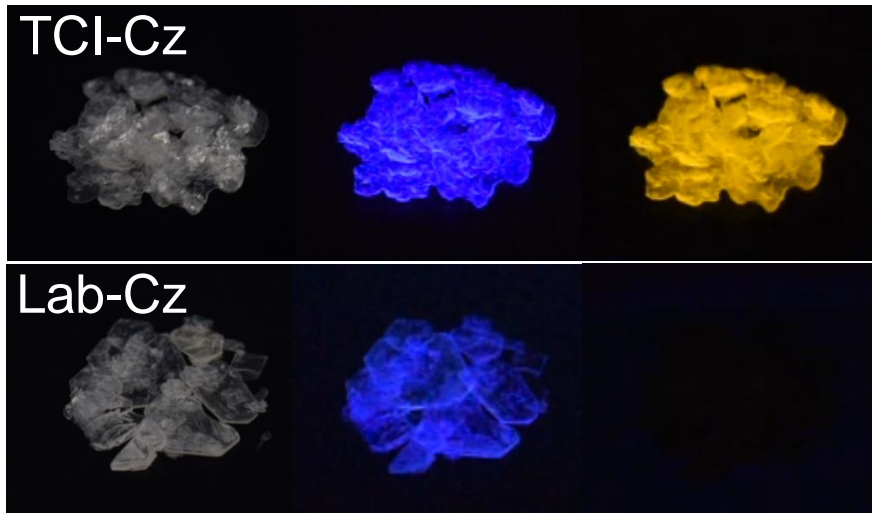
379 The data that support the findings of this study are available from C.C. and L.B. upon reasonable request. X-ray  
380 crystallographic data for structures reported here have been deposited in the Cambridge Crystallographic Data  
381 Centre (CCDC), under deposition numbers CCDC 1953802 to 1953811 and 2019581 to 2019589. These data can be  
382 obtained free of charge from the Cambridge Crystallographic Data Centre *via* [www.ccdc.cam.ac.uk/data\\_request/cif](http://www.ccdc.cam.ac.uk/data_request/cif).

## 383 References

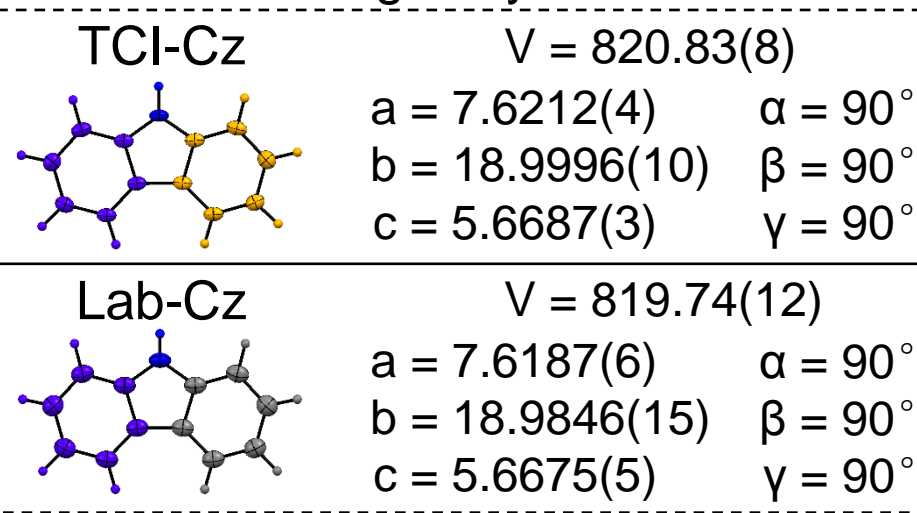
- 384 29. Ullah, E., McNulty, J. & Robertson, A. Highly chemoselective mono-Suzuki arylation reactions on  
385 all three dichlorobenzene isomers and applications development. *Eur. J. Org. Chem.* **2012**, 2127-2131  
386 (2012).
- 387 30. Yang, L., Zhang, Y., Zou, X., Lu, H. & Li, G. Visible-light-promoted intramolecular C-H amination  
388 in aqueous solution: synthesis of carbazole. *Green Chem.* **20**, 1362-1366 (2018).

389

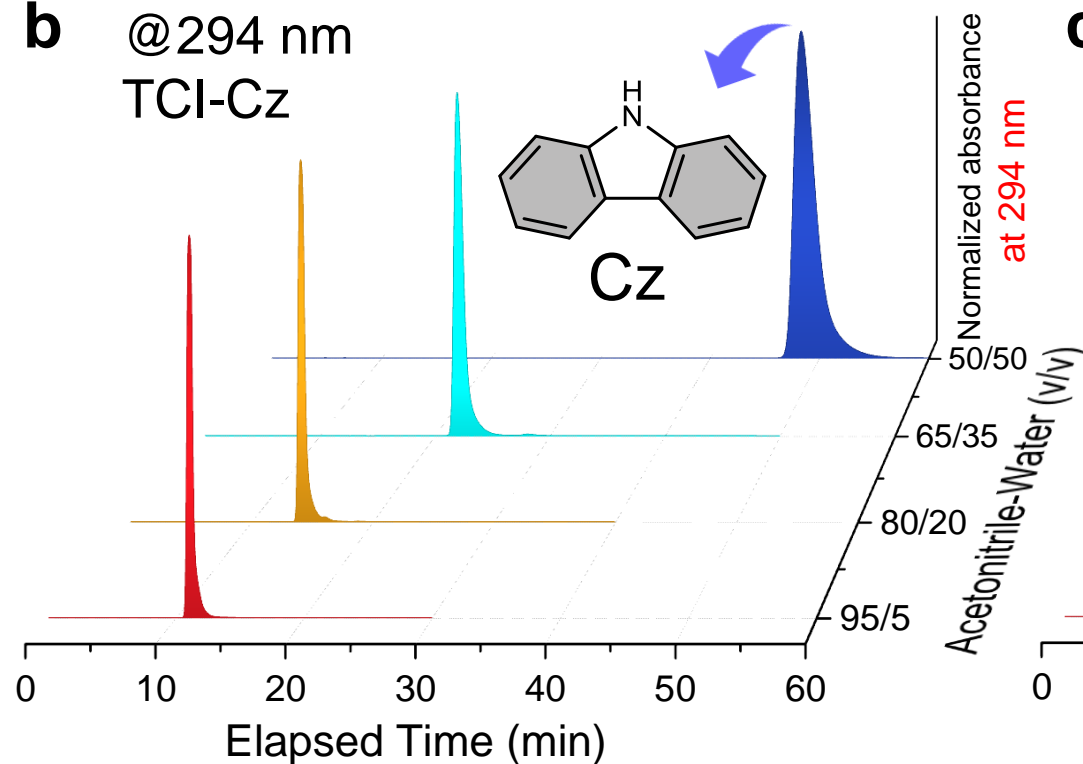
**a** Daylight 365 nm ON 365 nm OFF



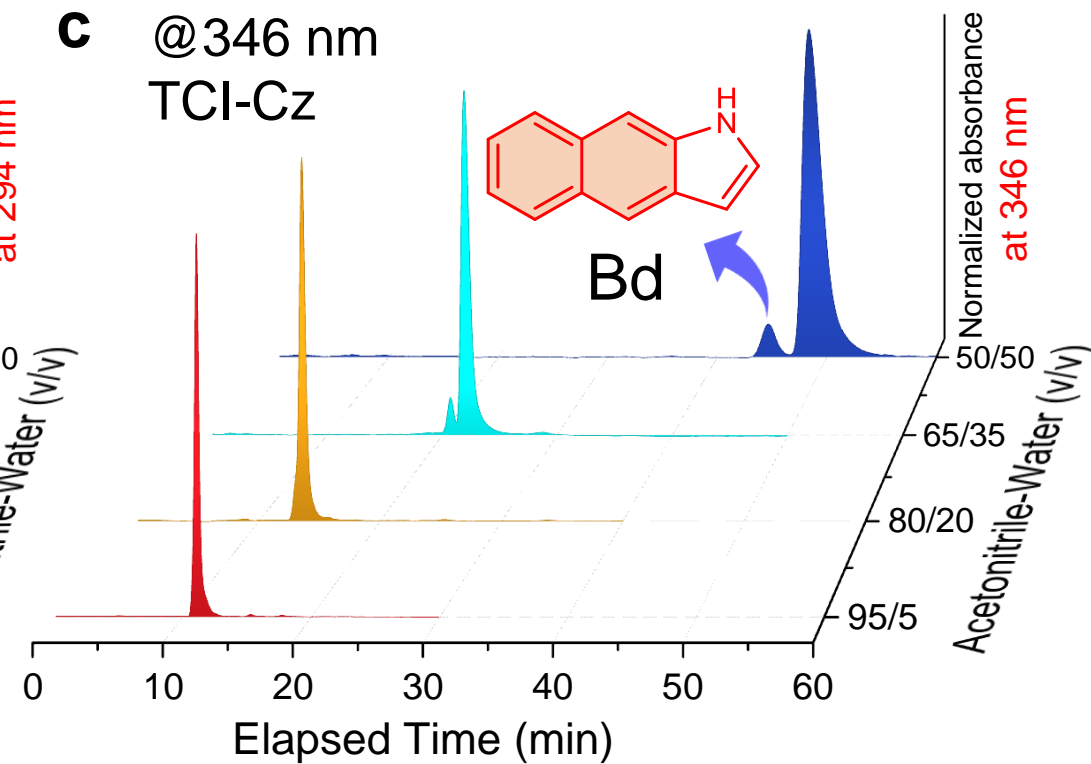
Single crystal

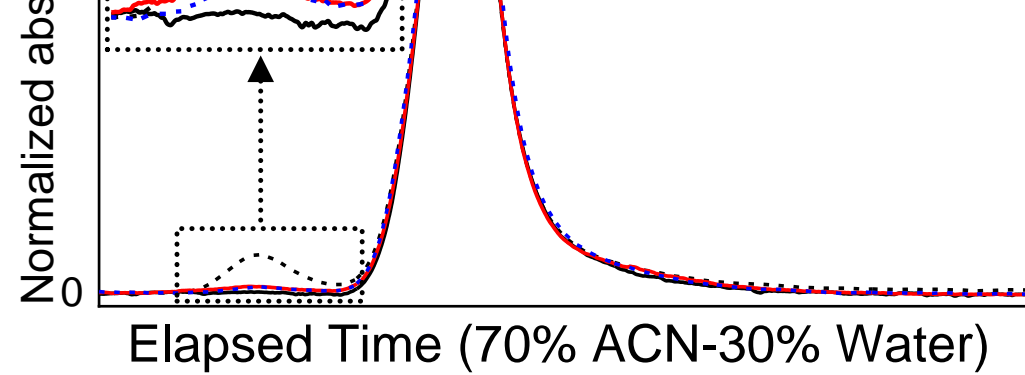
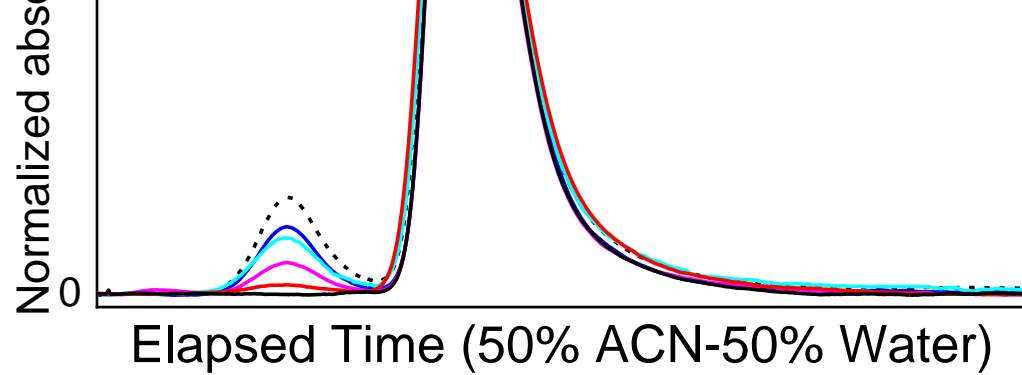


**b** @294 nm  
TCI-Cz

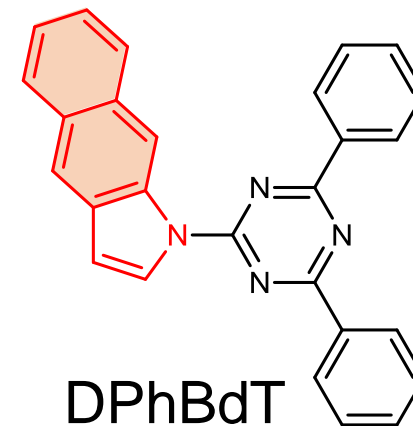
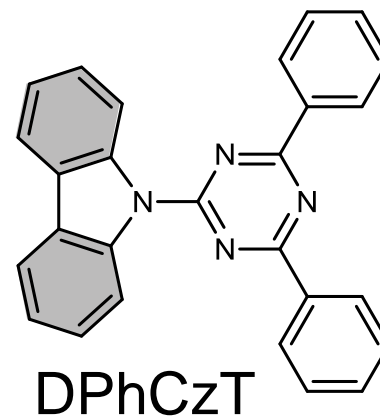
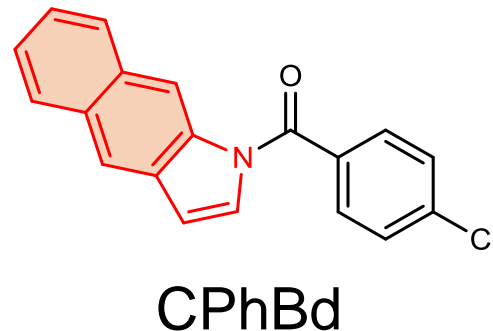
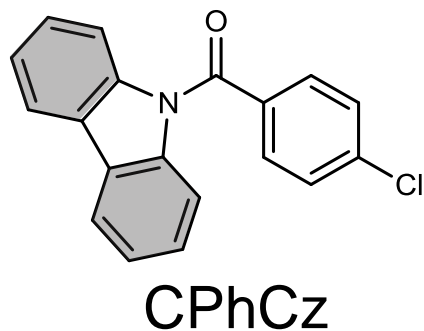


**c** @346 nm  
TCI-Cz





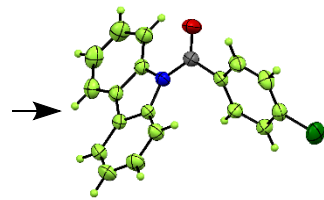
**c**



**d** Daylight      365 nm **ON**      365 nm **OFF**



Single crystal

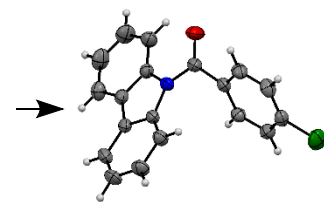


$$V = 1456.74(6)$$

$$a = 11.6461(3) \quad \alpha = 90^\circ$$

$$b = 10.0953(2) \quad \beta = 94.061(1)^\circ$$

$$c = 12.4215(3) \quad \gamma = 90^\circ$$



$$V = 1454.2(2)$$

$$a = 11.6304(11) \quad \alpha = 90^\circ$$

$$b = 10.0886(9) \quad \beta = 94.065(3)^\circ$$

$$c = 12.4251(11) \quad \gamma = 90^\circ$$

